Bremsstrahlung SPECT/CT

14

Stephan Walrand and Michel Hesse

14.1 Introduction

The first bremsstrahlung imaging was performed early in 1966 by Simon et al. [1, 2] using a rectilinear scanner following a liver radioembolization via the hepatic artery with ^{90}Y loaded 15-μm-diameter microspheres. Although of very low quality, this imaging already provided the main information: the carcinoid tumours were well preferentially targeted (Fig. 14.1).

The first use of an Anger camera for bremsstrahlung imaging was reported by Kaplan et al. in 1985 [3] for ^{32}P. Since the nineties, bremsstrahlung imaging is widely performed in clinical routine for post-therapy check using beta emitter, such as ^{90}Y synovectomy or ^{90}Y liver radioembolization. While medical publications about bremsstrahlung imaging are sparse up to the first decade of the twenty-first century, they significantly increased during the last decade (Table 14.1). This is to be linked to the expanded amount of performed ^{90}Y liver radioembolizations and developments of (faster) Monte-Carlo (MC) numerical methods to improve bremsstrahlung SPECT reconstructions.

Recently, Lhommel, Walrand et al. showed that the low positron emission of ^{90}Y can be usefully imaged by PET after liver radioembolization [4, 5] and after ^{90}Y-DOTATOC therapy as well [6]. Although giving final images a little bit noisier than bremsstrahlung SPECT, pure commercial TOF-PET systems directly provide good spatial resolution and quantification accuracy in ^{90}Y imaging. On the contrary, to achieve similar quality, bremsstrahlung SPECT requires sophisticated reconstruction or acquisition software not yet commercially available [7–9]. Those features explained the increasing use of PET to image ^{90}Y in place of bremsstrahlung SPECT at the begin of last decade (Table 14.1).

However, PET modality is not always easily accessible and as ^{32}P and ^{89}Sr do not own any usable isotope emitting γ rays which could be imaged, bremsstrahlung SPECT remains of paramount importance, as shown by the renewed interest in the last years (Table 14.1).

14.2 Bremsstrahlung SPECT Issues

Accurately imaging ^{90}Y, ^{32}P or ^{89}Sr with a γ camera is one of the most challenging topics in nuclear medicine. The bremsstrahlung X-rays are spread along a continuous spectrum extending to energies up to the maximal beta energy emission, i.e. 2.3 MeV, 1.7 MeV and 1.5 MeV for ^{90}Y, ^{32}P and ^{89}Sr, respectively. The maximal energy usable by γ camera owning a mechanical collimator, such as Anger or CZT cameras, is limited to

S. Walrand (✉) · M. Hesse
Nuclear Medicine, Université Catholique de Louvain, Brussels, Belgium
e-mail: stephan.walrand@uclouvain.be; michel.hesse@uclouvain.be

H. Ahmadzadehfar et al. (eds.), *Clinical Applications of SPECT-CT*,
https://doi.org/10.1007/978-3-030-65850-2_14

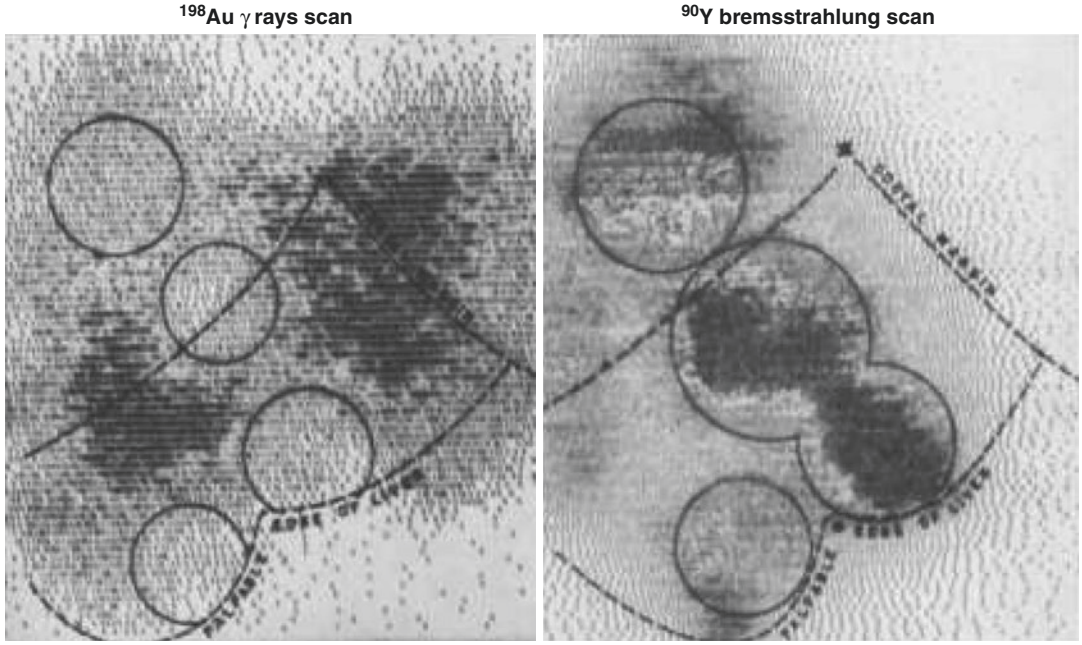

Fig. 14.1 Tumours appear cold in the diagnostic scan using ^{198}Au-chloride (1 μm-diameter) injected intravenously and trapped in the reticuloendothelial cells of the liver. (Figure reprinted from [2] with permission of the Radiological Society of North America)

Table 14.1 Sorted articles counts obtained from https://pubmed.ncbi.nlm.nih.gov/ when searching the combination (bremsstrahlung AND (SPECT OR SPET OR PET OR planar OR imaging OR whole-body)) in title/abstract

Year	89Sr	32P		90Y		90Y
		Planar	SPECT	Planar	SPECT	PET
<2007	3	3	3	7		
2007				2	1	
2008					2	
2009				1	3	1
2010	1	1		1	2	3
2011	1			2	4	6
2012	3		2	3	4	7
2012	4		2	3	7	2
2013	3		1	1	11	9
2014	1		1	1	7	7
2015				1	6	3
2016					10	9
2017	1		1	2	3	3
2018			2		11	5
2019				2	6	
2020					8	4

about 0.5 MeV. As a result, all acquisitions using such cameras are inevitably corrupted by high-energy X-rays scattering down into the acquisition energy window.

This high-energy X-rays down scattering contamination includes five different effects (Fig. 14.2): (1) the scattering inside the patient body, (2) the scattering through a collimator septa (usually called penetration), (3) the scattering from a collimator septa, (4) the lead fluorescence K_α and K_β emissions, (5) the back-scattering from the PMT, electronic boards and lead housing of the camera.

Although less frequent, some X-ray paths can include several of the sub-cited effects. Lastly, the β range in the patient also slightly alters the final spatial resolution.

Monte-Carlo simulations allow assessing the individual contributions to the total X-rays producing a photoelectric effect in the camera crystal [10] (Fig. 14.3). Note that contrary to conventional γ emitters, the primary photons represent only a small part of the total detected counts. The most favourable ratio is obtained around 100 keV explaining why the 50 → 150 keV energy window is often chosen [10, 11]. A medium energy general purpose (MEGP) parallel hole collimator is a good choice to reduce the collimator penetration. However, even with this energy window and collimator choice, spatial resolution and quantification accuracy of bremsstrahlung SPECT remain low. Different approaches are proposed to improve this situation: physical effects modelling and adapted collimator design.

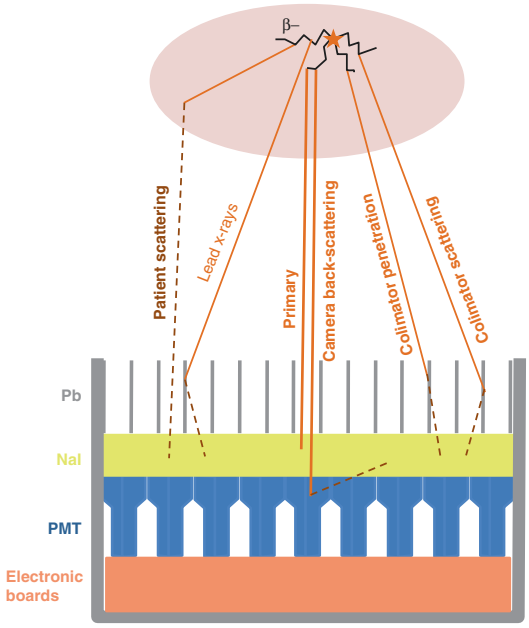

Fig. 14.2 The different X-rays paths producing a photoelectric effect in the camera crystal

14.3 Intra-Patient Scatter and Collimator-Detector Response Modelling

With the increasing speed of the computer stations, most tomographic reconstructions in nuclear medicine are nowadays performed using the iterative algorithm OSEM, an accelerated version of the EM-ML. Compared to analytical reconstruction, such as FBP, these iterative algorithms have the benefit to correctly account for the Poisson nature of the statistical noise present in radioactive counts measurement and to avoid apparition of negative voxel artefacts. In addition, iterative algorithms can reconstruct any tomographic acquisition setups, i.e. all physical effects introduced in the projection step of the

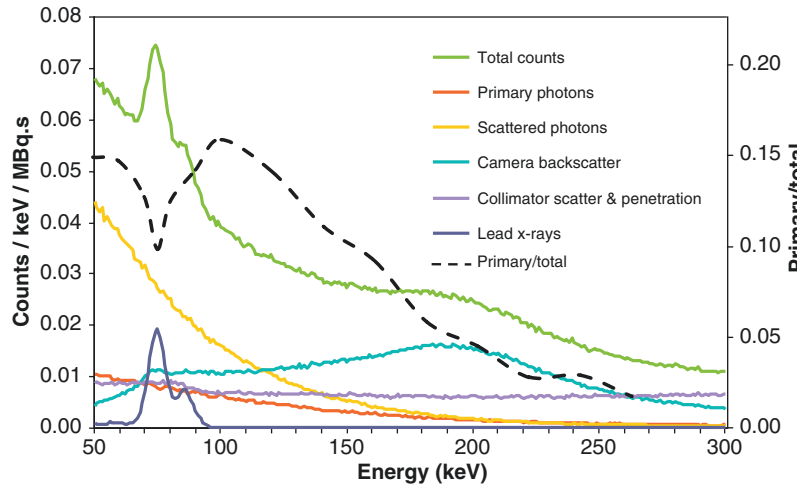

Fig. 14.3 ^{90}Y X-ray energy spectra according to photon origin for a point source 5 cm deep in water cube, MEGP collimation, 3/8 in. thick NaI, computed by Monte-Carlo simulation. Courtesy of Dr. S Heard. The primary to total counts curve (dashed black curve) was added by the author of the present chapter

iterative loop will be corrected during the reconstruction process. The state of the art in bremsstrahlung SPECT is thus to model the different X-ray paths during this projection step. However, for the time being an exact modelling of these effects lead to reconstruction time incompatible with the daily SPECT routine.

Minarik et al. [12] built a pre-calculated collimator-detector response (CDR) table by Monte-Carlo simulation and modelled the scatter into the object using the effective source scatter estimation (ESSE) method [13]. The modelling was performed for a 105–195 keV acquisition window in order to avoid the lead fluorescence X-rays contamination. This model was incorporated into the OSEM reconstruction algorithm. Evaluation in an abdominal phantom showed a quantification accuracy of 8.5% for the liver activity. Accuracy in lesions activity measurement was not assessed.

This group applied their correction method in three patients receiving high-dose ^{90}Y radioimmunotherapy [14]. The patients were imaged at 1, 24, 48, 72, 144, 166 h by SPECT/CT after a pre-therapeutic injection of 300 MBq of ^{111}In-ibritumomab. Patients received a ^{90}Y-ibritumomab activity computed to deliver 12 Gy to the liver based on the pharmacokinetics measured with the ^{111}In SPECT/CT and were imaged at the same time points post injection by bremsstrahlung SPECT/CT. The absolute relative differences between organ absorbed dose computed from ^{111}In and ^{90}Y SPECT/CT were 8.8 ± 13.7, 8.9 ± 4.0 and 51.7 ± 18.9 (mean ± std in %), for the liver, kidneys and lungs, respectively. This showed that this bremsstrahlung SPECT/CT correction method can be used for the body region below the lungs: for the time being, the ESSE method does not account for tissues density variation, such as present in the slices crossing the lungs.

Elschot et al. [15] developed a quantitative Monte-Carlo based SPECT reconstruction for ^{90}Y applications. They implemented a Monte-Carlo simulator to model the photon attenuation and scatter for the full ^{90}Y spectrum in the projection step, while pre-calculated convolution kernels were used for the collimator-detector response. Using a 50–250 keV energy window, they obtained quantification improvements compared to standard clinical SPECT-CT reconstructions for NEMA image quality phantom, and results close to PET-CT for a small set of patients after radioembolization with ^{90}Y resin spheres.

In order to improve the count rate for applications where the activity is modest, such as ^{90}Y radioimmunotherapy, Rong et al. [16] computed by Monte-Carlo the CDR and ESSE for the wide 100–500 keV acquisition window. The computation was performed using separate treatment of photons in various energy ranges and in various logical categories. Evaluation in an elliptical phantom containing three spheres of 5.5 cm, 3.3 cm and 1.5 cm-diameter, with specific activity ten-, ten- and 20-fold that of the surrounding background, showed a quantification accuracy of 7%, 9.7% and 10.2%, respectively.

To better take into account the energy dependence of photon–matter interaction probabilities and to simplify scatter corrections, Siman et al. [17] adapted the standard multi energy window approach to correct ^{90}Y SPECT-CT images for scatter. After splitting the 70–410 keV energy range into six windows whose widths were selected to enable a single attenuation coefficient use per window, they determined from phantoms the 90–125 keV and 310–410 keV ranges to be the best windows for imaging and scatter respectively. The scaling factor to multiply the scatter image was estimated from planar acquisitions of patients. This approach, while improving image quality and quantification, is strongly dependent on the camera and collimator used, and approximate as the scatter factor was averaged over different patients.

Dewaraja et al. [18] made use of Monte-Carlo only to estimate the scatter of photons, that they combined with a 3D OSEM reconstruction with an analytic projector for ^{90}Y SPECT-CT. Using a single energy window of 105–195 keV and a high-energy collimator, they showed that two iterations for the scatter estimation were enough, allowing a reduction of the reconstruction time to about 40 min. They so better recovered the activity in a liver/lung phantom, with values of 86%, 104% and 104% for the recovery in the intrahe-

patic lesions, normal liver and lungs respectively. They similarly observed an increase of the lesion to liver concentration with their MC reconstruction for patient studies compared to standard SPECT-CT reconstructions.

More recently Chun et al. [19] proposed an interesting approach of joint spectral reconstruction for quantitative ^{90}Y SPECT imaging. They used multiple narrow acquisitions windows with multi-band forward modelling. The latter has the advantage to permit a better modelling of energy dependent physics like using more adequate attenuation coefficients in place of only one corresponding to the mid-range energy. The former allowed the authors to extract and combine activity data from the different energy window acquisitions to improve the reconstructed image. They also presented an accelerated algorithm using energy subsets similarly to the angular subsets in OSEM. MC simulations were used at every five iterations to estimate the scatter components without impacting too much the reconstruction time. With this new algorithm they reached faster convergence of the recovery coefficients in phantom studies than with single spectral/single energy window and multi spectral/single energy window reconstructions. The proposed method has also the advantage to implement matched forward and backward projectors, inducing better convergence stability, unlike most of developed reconstruction algorithms where MC scatter and collimator modelling is only incorporated in the forward projector.

Another physical characteristic seldom considered is the dependence of the bremsstrahlung generation with respect to the tissue types. Lim et al. [20] modelled by Monte-Carlo the bremsstrahlung generation probabilities according to the tissue. With their adapted reconstruction algorithm, they showed on phantom acquisition and simulations improved estimations of ^{90}Y activities in tissues differing from water. Unfortunately that study did not include absolute quantification, nor patient imaging.

Very recently, Xiang et al. [21] made use of latest developments in artificial intelligence to train a deep convolutional neural network from ^{90}Y SPECT projections and CT attenuation maps to produce scatter projections. The training set was made of simulated numerical phantom data for which actual scatter component is known. With that approach they obtained image quality and contrast recovery similar to MC scatter estimation but in much less time. This still requires developments in training data and quantitative validations, but could pave the way to better bremsstrahlung SPECT-CT reconstructed images in clinical routine.

However, in medical imaging it is always profitable to improve the hardware performance in order to acquire the right events, rather than to correct for the contaminating events afterwards. Indeed, this last solution inevitably results in a higher noise level regarding the statistical nature of primary and contaminating photon. Amazingly, other choices of collimators than MEGP have been considered only very recently.

14.4 Choice of Collimators Better Adapted to Bremsstrahlung Imaging

Van Holen et al. [8] proposed the use of a rotating slat collimator that owns a much higher geometric efficiency than a parallel hole collimator. As a result the relative importance of septal penetration is reduced, resulting in better contrast to noise ratio. Note, that regarding only the primary X-rays, the high geometric efficiency improvement of the rotating slat collimator is counterbalanced by less information provided about the X-ray coming direction. Data publication in a full paper is still pending.

Walrand et al. [9] used a conventional thyroid dedicated medium energy pinhole (MEPH) collimator in bremsstrahlung SPECT in purpose of ^{90}Y liver radioembolization check. Scattering inside the phantom was modelled using an adaptation of an effective scatter model previously developed for ^{99m}Tc [22], similar and anterior to ESSE [13]. Compared to parallel hole collimators, the high-energy X-rays can hit lead material mostly only on the external side of the pinhole collimator housing (Fig. 14.4a). As a result, the lead fluorescence and scattering X-rays cannot

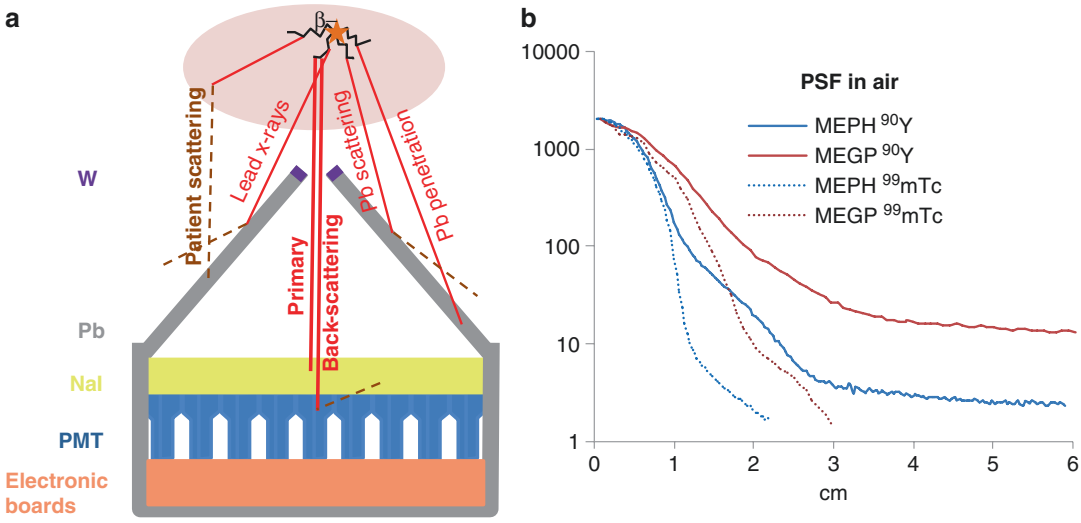

Fig. 14.4 (**a**) reduction of the disturbing X-rays paths contributing to the total crystal photoelectric counts. (**b**) point spread function (PSF) comparison of a ^{90}Y and ^{99m}Tc point source in air with a MEPH and MEGP collimator using a 1/2 in. thick NaI GE 400 AC camera with a 50–150 keV acquisition window. ^{99m}Tc PSF approximates the PSF of the primary photons in the ^{90}Y acquisition

reach the crystal as the collimator housing thickness (2 cm) is sufficient to significantly reduce penetration. Disturbing penetration-scattering can only occur on the small tungsten insert, the fluorescence X-ray emissions of which are located below 10 keV [23]. These features improve the primary to total count ratio (Fig. 14.3). The comparison between ^{90}Y and ^{99m}Tc radial profile in air (Fig. 14.4b) shows that using a 50–150 keV acquisition window the primary photons represent 68% and 31% of the total detected photons for MEPH and MEGP collimators, respectively.

Evaluation in cold and hot spheres phantom [9] showed that MEPH SPECT provided quantification accuracy similar to that of TOF-PET, but with significantly less noise. Helical MEPH SPECTs of a realistic liver radioembolization phantom were also acquired and showed that reproducible accurate activity quantification can be obtained in 1 min acquisition time (relative deviation of healthy liver compartment: $10 \pm 0.1\%$).

Gupta et al. [24] showed the feasibility of real-time visualization of iron-labelled microspheres delivery during liver SIRT in rabbits using MRI. In this paper, cosigned by R. Salem, the authors concluded: "Although quantitative in vivo estimation of microsphere biodistribution may prove technically challenging, the clinical effect could be enormous, thus permitting dose optimization to maximize tumour kill while limiting toxic effects on normal liver tissues." However, human liver SIRT appears quite incompatible with MR: the X-ray angiographic imager will difficultly be implemented around the MR table, and the long duration of liver SIRT, that can overpass 2 h for challenging arterial trees, is not supportable by most of MRI agenda.

14.5 Current Bremsstrahlung SPECT-CT Routine Applications

For the time being, dedicated bremsstrahlung acquisition hardware or reconstruction software are not commercially available, and most bremsstrahlung routine SPECT-CT are performed without any special correction. This is not a major problem as far as they are intended to post-therapy visual check. However, users have to be

very cautious when performing quantitative measurement on standard acquisition-reconstruction of bremsstrahlung X-rays.

^{90}Y radio-synovectomy has been the main application of bremsstrahlung routine imaging since 30 years. However, regarding to the small size of the synovial compartment, the higher spatial resolution of PET system is a major benefit to perform an optimal check of this therapy [25]. In addition, as the activity is located into a small volume, noise issues are very limited.

Liver radioembolization with ^{90}Y loaded microspheres by catheterization through the hepatic artery is an emerging treatment for primary and metastatic liver cancer. However selective radioembolization fully confined in the targeted hepatic artery branch is a challenging operation. Microspheres can be spread in the arterial tree along a different pattern than those of the macro-aggregates or of the contrast agent (see "choice of a surrogate" in chapter "SPECT for dosimetry") leading to adverse effects [26].

Until the possibility of tracking the microspheres delivery during the catheterization, it is thus of paramount importance to check the microsphere distribution post therapy in order to take the appropriate cares to reduce the side effects in case of activity delivered in critical tissues. Ahmadzadehfar et al. [27] evaluated the significance of bremsstrahlung SPECT/CT in the prediction of extrahepatic side effects after 188 radioembolizations with ^{90}Y-microspheres. They observed a dramatic improvement of the sensitivity and of the positive predictive value of SPECT/CT (87% and 100%) compared to SPECT alone (13% and 8%), leading to a final accuracy of 99%. The two cases shown in Fig. 14.5 clearly illustrate the benefit of this co-acquisition.

Peptides receptor targeted therapies are usually performed in several cycles in order to limit kidneys toxicity [28]. Fabbri et al. [29, 30] evaluated on anatomical phantom the feasibility to perform organs dosimetry after each ^{90}Y-DOTATOC cycle in order to optimize the

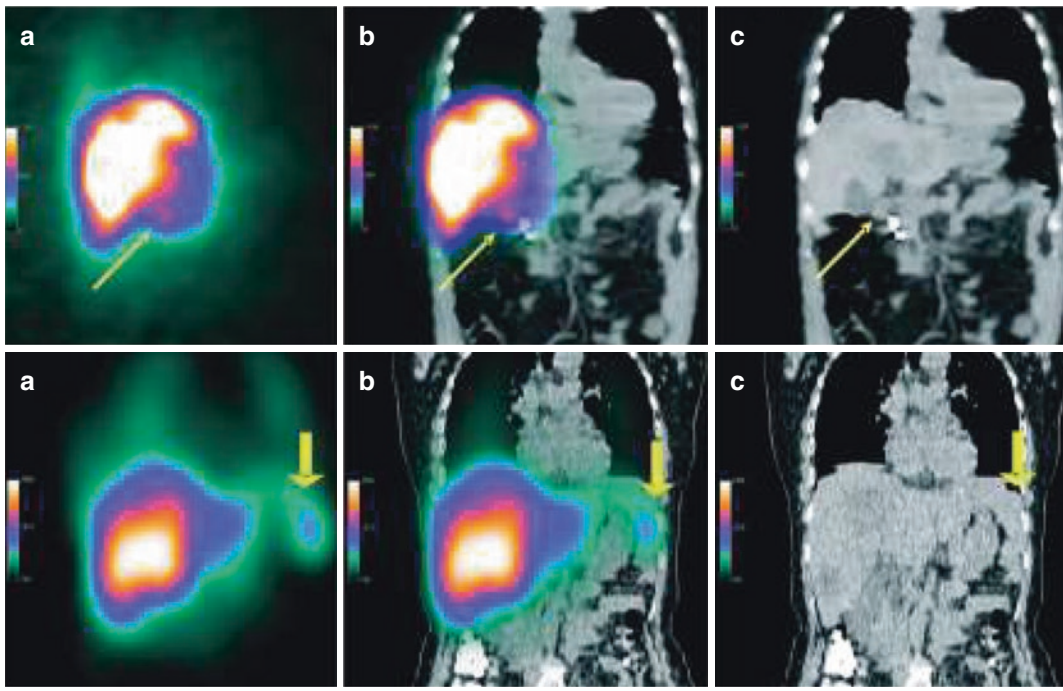

Fig. 14.5 ^{90}Y bremmstrahlung SPECT (**a**)/CT (**c**) co-registration (**b**). Top row: Patient with a focal activity in the duodenum as shown by the SPECT-CT co-registration (thin yellow arrow). Patient received a daily pump inhibitor, but got a duodenal ulcer without active bleeding confirmed by gastroduodenoscopy. Bottom row: Patient with a suspicious focal activity in SPECT (thick yellow arrow), but proved to be hypertrophied left liver lobe in the SPECT-CT co-registration. (Reprinted from [27] with permission of Springer-Verlag)

activity to be injected in the next one. They showed on a phantom that, using the standard reconstruction software of the SPECT/CT system, but with calibration factors depending on the lesion or organ volume measured on the CT, it was possible to access the dosimetry within an accuracy of 10%. Calibration factors ranged from 0.4 to 1.3 for the tissue ranging from 8 to 150 mL. However this method does not correct for the cross scattering organ contamination which can be problematic for the activity quantification in kidneys with close bowel or tumour surrounding activities. Studies on phantom of various sizes and of various activity distributions are thus suitable to further assess its accuracy.

Following a clinical study with ^{90}Y Zevalin to treat lymphomas, Shiba et al. [31] analysed the impact on ^{90}Y bremsstrahlung SPECT images of the presence of residual ^{111}In from pre-therapeutic evaluation. Their results indicated that ^{111}In is still prevalent in the post-therapeutic image 1 week after its injection. Combined with the limited image quality of ^{90}Y bremsstrahlung SPECT, the authors recommend the use of PET/CT imaging for that kind of application.

14.6 Dose–Response Studies Based on Bremsstrahlung SPECT

With the speed-up development in the last decade of computer tools that improve the image quality of bremsstrahlung SPECT/CT, several groups started performing dosimetric studies based on bremsstrahlung and were able to extract dose–response relationships.

Kappadath et al. [32] performed voxel dosimetry based on bremsstrahlung SPECT/CT on patients treated for hepatocellular carcinoma by ^{90}Y-radioembolization with glass microspheres. From SPECT/CT iterative reconstructions including attenuation, scatter and collimator modelling, they obtained a correlation between dose metrics and mRECIST response, with a mean dose of 160 Gy and a mean biological effective dose of 214 Gy for 50% probability of response, giving positive predictive value of 70% and negative predictive value of 62%.

Piasecki et al. [33] studied the dose–response for colorectal liver metastases after ^{90}Y radioembolization. They obtained relationships between predicted tumour doses from ^{99m}Tc-MAA SPECT/CT and responses, but not when looking at the actual ^{90}Y tumour absorbed doses evaluated from ^{90}Y bremsstrahlung SPECT/CT. This may be in part due to the use of standard iterative reconstruction that does not include dedicated scatter or collimator modelling. Using standard manufacturer reconstruction without specific corrections. Schobert et al. [34] were able to obtain dose–response relationship in HCC after ^{90}Y radioembolization, but not for non-HCC lesions, by performing bremsstrahlung SPECT/CT with low energy high resolution collimators and standard iterative reconstruction.

These studies should be looked at as early and promising examples of feasibility of dosimetric analyses, but many developments and validations are still needed before accurate dosimetry can be obtained from bremsstrahlung SPECT/CT imaging.

14.7 Perspectives: New Detectors Better Adapted to Bremsstrahlung Imaging

Cadmium zinc tellurium (CZT) detectors, although still expensive, are emerging in dedicated cardiac SPECT systems [35] where their compactness and absence of dead edge area allows to build area of independent detectors all focussing to the heart. With the future decrease in manufacturing cost, CZT will become more and more used for general purpose γ cameras in order to profit of its better energy resolution [36]. Indeed, for γ emitters, a better energy resolution allows to narrow the acquisition window around the photoelectric peak which reduces the detection of γ rays scattered inside the patient body and results in a better image contrast. These CZT cameras should also be better adapted to bremsstrahlung imaging as the quantity of medium Z material (glass, iron, copper), present between the γ detection area and the detector housing, and which backscatter the high-energy X-rays, will be reduced. The camera housing should prefera-

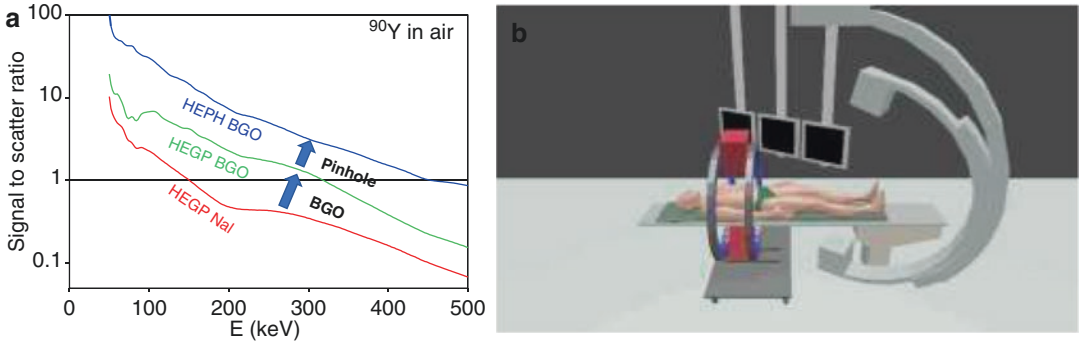

Fig. 14.6 (**a**) Monte-Carlo simulations of detected energy spectra for a ^{90}Y source in air in front of a gamma camera including a NaI crystal and equipped with a high-energy general purpose (HEGP) collimator (red curve), including a BGO crystal and equipped with a HEGP (green curve) or a high-energy pinhole (HEPH) collimator (blue curve) [37]. The curves represent the ratio of geometric counts to scattered counts with respect to the detected ray energy. (**b**) Illustration of a mobile dual head BGO-camera equipped with HEPH collimators to be used directly in the catheterization room to image the microspheres distribution and help the radiologist in optimizing the patient dose

bly be made in tungsten which has its fluorescence X-rays emission around 10 keV [23].

Recently Walrand et al. [37] simulated the detected energy spectra for ^{90}Y to illustrate the impact of scattered bremsstrahlung rays. Figure 14.6a represents the signal to scatter ratio, i.e. the total counts coming from the geometric X-rays to those coming from scattered X-rays, with respect to the detected X-rays energy. The signal clearly increases when the NaI crystal is replaced by a BGO crystal, and again when the high-energy parallel hole collimator is replaced by a pinhole collimator.

The simulation of the BGO-pinhole camera shows that the ratio is above 1 (geometric X-rays outnumber scattered ones) in almost all the 50–500 keV energy range. This opens the way to the development of the continuous energy tomography where the detected X-rays energy provides additional information for the image reconstruction similarly to the detector angle in conventional SPECT imaging.

This could be used to optimize the patient dose directly in the catheterization room (Fig. 14.6b). After a first injection of microspheres (^{90}Y, ^{166}Ho or ^{32}P), a BGO-pinhole camera is moved around the patient and a 2 min scan provides data that are treated by a dosimetric software. From its results the radiologist can estimate if and how much activity can still be injected in the patient. The procedure can be iterated until optimal activity has been injected.

Compton cameras are under intensive development in physics labs [27]. Similarly to PET, the purpose of Compton camera is to get free of the mechanical collimator in order to improve both the spatial resolution and the sensitivity as well. Applied to bremsstrahlung imaging, Compton camera will be free of any collimator disturbing effects. In Compton camera the photon is detected in two distant planes, i.e. the Compton and the scintillation detector. Thus, measuring the time detection sequence between these two planes will also allow discrimination between primary and backscattered photons. Lastly, sensitivity of Compton camera increases with rays energy, and acquisition with very wide energy window could be used to further increase the sensitivity.

14.8 Conclusions

With the increasing accessibility to PET systems, ^{90}Y PET imaging will likely remain the gold standard for ^{90}Y imaging. However the increasing amount of performed ^{90}Y therapies will see the continuing developments and improvements of ^{90}Y bremsstrahlung SPECT imaging, especially on the software side with better corrections to

achieve imaging quality similar to PET. Moreover, bremsstrahlung SPECT will remain the only way to image ^{32}P and ^{89}Sr, two isotopes regaining interest in radiotherapy. In addition, use of a dedicated pinhole collimator could allow performing fast bremsstrahlung SPECT quantification during liver radioembolization. Soon, the emerging CZT detectors should further improve bremsstrahlung SPECT. In a distant future, Compton camera could revolutionize this imaging modality.

References

1. Simon N, Feitelberg S, Warner RRP, Greenspan EM, Edelman S, Baron MG. External scanning of internal beta-emitters. J Mt Sinai Hosp. 1966;33:365–70.
2. Simon N, Feitelberg S. Scanning Bremsstrahlung of Yttrium-90 microspheres injected intra-arterially. Radiology. 1967;88:719–24.
3. Kaplan WD, Zimmerman RE, Bloomer WD, Knapp RC, Adelstein AJ. Therapeutic intraperitoneal 32P: a clinical assessment of the dynamics of distribution. Radiology. 1981;138:683.
4. Lhommel R, Goffette P, Van den Eynde M, Jamar F, Pauwels S, Bilbao JI, Walrand S. Yttrium-90 TOF PET scan demonstrates high-resolution biodistribution after liver SIRT. Eur J Nucl Med Mol Imaging. 2009;36(10):1969.
5. Lhommel R, van Elmbt L, Goffette P, Van den Eynde M, Jamar F, Pauwels S, Walrand S. Feasibility of Yttrium-90 TOF-PET based dosimetry in liver metastasis therapy using SIR-spheres. Eur J Nucl Med Mol Imaging. 2010;37(9):1654–62.
6. Walrand S, Jamar F, van Elmbt L, Lhommel R, Bidja'a Bekonde E, Pauwels S. 4-Step renal dosimetry dependent on cortex geometry applied to 90Y peptide receptor radiotherapy: evaluation using a fillable kidney phantom imaged by 90Y PET. J Nucl Med. 2010;51:1969–73.
7. Walrand S, Flux GD, Konijnenberg MW, Valkema R, Krenning EP, Lhommel R, Pauwels S, Jamar F. Dosimetry of yttrium-labelled radiopharmaceuticals for internal therapy: (86)Y or (90)Y imaging? Eur J Nucl Med Mol Imaging. 2011;38(1):S57–68.
8. Van Holen R, Staelens S, Vandenberghe S. SPECT imaging of high energy isotopes and isotopes with high energy contaminants with rotating slat collimators. Med Phys. 2009;36:4257–67.
9. Walrand S, Hesse S, Demonceau G, Pauwels S, Jamar F. Yttrium-90 labeled microspheres tracking during liver selective internal radiotherapy by bremsstrahlung pinhole SPECT: feasibility study and evaluation in an abdominal phantom. EJNMMI Res. 2011;1:32.
10. Heard S, Flux GD, Guy MJ, Ott RJ. Monte Carlo simulation of ^{90}Y Bremsstrahlung imaging. IEEE Nucl Sci Symp Conf Rec. 2004;6:3579–83.
11. Siegel JA. Quantitative Bremsstrahlung SPECT imaging: attenuation-corrected activity determination. J Nucl Med. 1994;35(7):1213–6.
12. Minarik D, Gleisner KS, Ljungberg M. Evaluation of quantitative (90) Y SPECT based on experimental phantom studies. Phys Med Biol. 2008;53:5689–703.
13. Frey EC, Tsui BMW. A new method for modeling the spatially variant, object-dependent scatter response function in SPECT. IEEE Nucl Sci Symp. 1996;2:1082–6.
14. Minarik D, Sjőgreen-Gleisner K, Linden O, Winga K, Tennvall J, Strand S-E, Ljungberg M. ^{90}Y Bremsstrahlung imaging for absorbed-dose assessment in high-dose radioimmunotherapy. J Nucl Med. 2010;51:1974–78.
15. Elschot M, Lam MGEH, van den Bosch MAAJ, Viergever MA, de Jong HWAM. Quantitative Monte Carlo-based ^{90}Y SPECT reconstruction. J Nucl Med. 2013;54:1557–63.
16. Ronga X, Du Y, Ljungberg M, Rault E, Vandenberghe S, Frey EC. Development and evaluation of an improved quantitative ^{90}Y bremsstrahlung SPECT method. Med Phys. 2012;39:2346–58.
17. Siman W, Mikell JK, Kappadath SC. Practical reconstruction protocol for quantitative ^{90}Y bremsstrahlung SPECT/CT. Med Phys. 2016;43:5093–103.
18. Dewaraja YK, Chun SY, Srinivasa RN, Kaza RK, Cuneo KC, Majdalany BS, Novelli PM, Ljungberg M, Fessler JA. Improved quantitative 90Y bremsstrahlung SPECT/CT reconstruction with Monte Carlo scatter modeling. Med Phys. 2017;44:6364–75.
19. Chun SY, Nguyen P, Phan TQ, Kim H, Fessler JA, Dewaraja YK, et al. Algorithms and analyses for joint spectral proposed an interesting approach of joint spectral image reconstruction in Y-90 bremsstrahlung SPECT. IEEE Trans Med Imaging. 2020;39:1369–79.
20. Lim H, Fessler JA, Wilderman SJ, Brooks AF, Dewaraja YK. Y-90 SPECT ML image reconstruction with a new model for tissue-dependent bremsstrahlung production using CT information: a proof-of-concept study. Phys Med Biol. 2019;63:115001.
21. Xiang H, Lim H, Fessler JA, Dewaraja YK. A deep neural network for fast and accurate scatter estimation in quantitative SPECT/CT under challenging scatter conditions. EJNMMI. 2020;47:2956–67.
22. Walrand SH, van Elmbt LR, Pauwels S. Quantitation in SPECT using an effective model of the scattering. Phys Med Biol. 1994;39(4):719–34.
23. X-ray Department. X-ray wavelengths for spectrometer. 4th ed. Boston, MA: General Electric Company; 1966.
24. Gupta T, Virmani S, Neidt TM, Szolc-Kowalska B, Sato KT, Ryu RK, Lewandowski RJ, Gates VL, Woloschak GE, Salem R, Omary RA, Larson AC. MR tracking of iron-labeled glass radioembolization microsphres during

transcatheter delivery to rabbit VX2 livers tumors: feasibility study. Radiology. 2008;249(3):845–54.
25. Barber TW, Yap KS, Kalff V. PET/CT imaging of ^{90}Y radiation synovectomy. Eur J Nucl Med Mol Imaging. 2012;39(5):917–8.
26. Riaz A, Lewandowski RJ, Kulik LM, Mulcahy MF, Sato KT, Ryu RK, et al. Complications following radioembolization with yttrium-90 microspheres: a comprehensive literature review. J Vasc Interv Radiol. 2009;29:1121–30.
27. Ahmadzadehfar H, Muckle M, Sabet A, Wilhelm K, Kuhl C, Biermann K, Haslerud T, Biersack HJ, Ezziddin S. The significance of bremsstrahlung SPECT/CT after yttrium-90 radioembolization treatment in the prediction of extrahepatic side effects. Eur J Nucl Med Mol Imaging. 2011;39:309–15.
28. Barone R, Borson-Chazot F, Valkema R, Walrand S, Chauvin F, Gogou L, Kvols LK, Krenning EP, Jamar F, Pauwels S. Patient-specific dosimetry in predicting renal toxicity with (90)Y-DOTATOC: relevance of kidney volume and dose rate in finding a dose-effect relationship. J Nucl Med. 2005;46:99S–106S.
29. Fabbri C, Sarti G, Agostini M, Di Dia A, Paganelli G. SPECT/CT 90Y-Bremsstrahlung images for dosimetry during therapy. Ecancermedicalscience. 2008;2:106.
30. Fabbri C, Sarti G, Cremonesi M, Ferrari M, Di Dia A, Agostini M, Botta F, Paganelli G. Quantitative analysis of 90Y Bremsstrahlung SPECT-CT images for application to 3D patient-specific dosimetry. Cancer Biother Radiopharm. 2009;24(1):145–54.
31. Shiba H, Takahashi A, Baba S, Himuro K, Yamashita Y, Sasaki M. Analysis of the influence of ^{111}In on ^{90}Y-bremsstrahlung SPECT based on Monte Carlo simulation. Ann Nucl Med. 2016;30:675–81.
32. Kappadath SC, Mikell J, Balagopal A, Baladandayuthapani V, Kaseb A, Mahvash A. Hepatocellular carcinoma tumor dose response after ^{90}Y-radioembolization with glass microspheres using ^{90}Y-SPECT/CT-based voxel dosimetry. Int J Radiat Oncol Biol Phys. 2018;102:451–61.
33. Piasecki P, Narloch J, Brzozowski K, Ziecina P, Mazurek A, Budzynska A, Korniluk J, Dziuk M. The predictive value of SPECT/CT imaging in colorectal liver metastases response after ^{90}Y-radioembolization. PLoS One. 2018;13:e0200488. https://doi.org/10.1371/journal.pone.0200488.
34. Schobert I, Chapiro J, Nezami N, Hamm CA, Gebauer B, Lin M, Pollak J, Saperstein L, Schlachter T, Savic LJ. Quantitative imaging biomarkers for Yttrium-90 distribution on bremsstrahlung single photon emission computed tomography after resin-based radioembolization. J Nucl Med. 2019;60:1066–72.
35. Slomka PJ, Patton JA, Berman DS, Germano G. Advances in technical aspects of myocardial perfusion SPECT imaging. J Nucl Cardiol. 2009;16(2):255–76.
36. Walrand S, Jamar F. Imaging in nuclear medicine. In: Giussani A, editor. Perspectives in nuclear medicine tomography: a physicist's point of view. Berlin: Springer; 2013.
37. Walrand S, Hesse M, Wojcik R, Lhommel R, Jamar F. Optimal design of Anger camera for bremsstrahlung imaging: Monte Carlo evaluation. Front Oncol. 2014;4:149.